

# 3D Segmentation for the Study of Cell Cycle Progression in Live *Drosophila* Embryos

Chinta Rambabu, Puah Wee Choo, Janos Kriston-Vizi and Martin Waser

Bioinformatics Institute, A\*STAR  
30 Biopolis Street, Matrix Building, Singapore 138671, Singapore

**Abstract.** We study the dynamics of cell division in live *Drosophila* embryos using fluorescent proteins and 3D time-lapse microscopy. Accurate segmentation of nuclei and mitotic chromosomes labeled by the live reporter histone-GFP is a prerequisite for subsequent tracking and quantitative object analysis. We propose an automated 3D segmentation method based on narrow band level sets that preserves the boundary of the cell nuclei and removes signals that are artifacts of live cell imaging. We introduce an improved 3D narrow band approach in the region shrinking and growing process for accurately segmenting the cell nuclei from background. The proposed method has been evaluated with the ground truth regarding the object level accuracy and segmentation quality. Both the object level accuracy and pixel accuracy of the proposed method are around 96% and 85% respectively. Our algorithm can robustly segment nuclei and chromosomes in different phase of the division cycle.

## 1 Introduction

Cell cycle regulation plays an important role in disease and development. *Drosophila* embryogenesis is an excellent model system to study the mechanics and regulation of cell division cycle in an intact multi-cellular organism [1]. The first 13 nuclear division cycles are synchronous and take place in a common cytoplasm shared by all nuclei. After completion of the syncytial blastoderm, cells form and all subsequent cell divisions happen within the confines of cell membranes. Fluorescence proteins, such as histone-GFP, in conjunction with 3D video microscopy can be applied to monitor cell cycle progression in living cells. Quantitative analysis of 3D image stacks can provide novel insights into the cell division cycle and its genetic regulation. However, computer vision tasks like feature extraction, quantification, classification and tracking are highly dependent on the accuracy of image segmentation.

Several automatic 3D segmentation methods [2–7] have been developed for segmentation of cell nuclei. The most common methods used for cell nuclei segmentation can be classified as watershed, model and active surface-based methods. Watershed-based methods [2] [3] are very popular for segmentation of merged nuclei. However, they are prone to over-segmentation and requiring complex postprocessing. Model-based segmentation method [4] has demonstrated highest segmentation accuracy but they rely on a *a priori* model of the expected nuclei morphology. Moreover, various

active surface based methods [5–7] have been proposed for nuclear segmentation. In the active surface-based methods, objects are represented as a smooth surface, which evolves with a speed force depending on the geometric property of the surface and the external energy. However, the active surface-based methods suffer from an inherent dependency on the initial seed. Various methods exist in the literature [2–7]; all of which have been developed under restricted environmental conditions and are motivated by specific application problem.

In 3D live microscopy, various factors, including uneven illumination due to limited depth penetration, photo-bleaching, poor signal-to-noise ratio (SNR), heterogeneity in the localization of fluorescent molecules and other artifacts can affect the performance of segmentation. In order to characterize the dynamic changes of nuclear and chromosomal morphology during the division cycles we propose a segmentation algorithm that has to meet the following requirements: (1) recognition of various shapes and textures in the different stages of interphase and mitosis, (2) recognition during different stages of development and (3) robustness of the object detection against fluorescence signals that are not associated with nuclei, e.g. lipid droplets. In this paper, we present a hybrid 3D segmentation method that aims to handle the above-mentioned challenges of nuclear segmentation. We also present experimental results and validation of the proposed method.

## 2 Hybrid 3D Segmentation Method

In this section, we describe an automated hybrid 3D segmentation approach that preserves the surfaces of cell nuclei and is also robust against imaging artifacts inherent to laser scanning confocal microscopy (LSM). The method is composed of a sequence of four major steps; namely preprocessing, background/foreground model, cell object detection and marker-based region growing (Figure 1). The detailed description of the major steps is provided next.

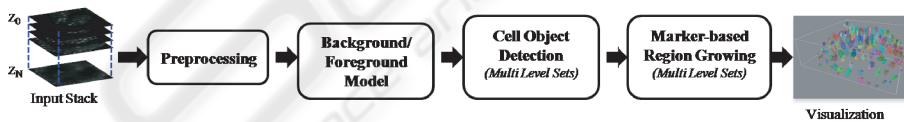


**Fig. 1.** Flow chart illustrating the major steps in the proposed method.

### 2.1 Image Acquisition

Cell nuclei and chromosomes in *Drosophila* embryos were labeled using the live fluorescence reporter histone H2Av-GFP [8]. Image acquisition was performed using an inverted Zeiss 5 Live laser scanning confocal microscope and a 63x N.A. 1.3 oil immersion lens. *Drosophila* embryos were dechorionated in 50% bleach and embedded in 1% agarose on a glass bottom dish. Image de-convolution was carried using the Huygens Professional, version 3.0.

## 2.2 Preprocessing

Serial optical sections produced by confocal microscopy tend to suffer from attenuation of fluorescence signals in deeper tissue layers. In order to compensate for uneven illumination within the same image stack, we use a simple method that normalizes pixel intensity relative to the optical slice which shows the highest mean intensity. Moreover, live cell imaging records signals that are not associated with nuclei or chromosomes. These can be due to auto-fluorescence or cytoplasmic histone-GFP containing lipid droplets [9]. Compared to cell nuclei, lipid droplets have a smaller size and differ both in mean and standard deviation of intensity. A series of median filters was used to alleviate the problem. However, variable window size filtering altered the shape of object boundaries and increased false detection rate. To overcome this problem, we introduced a novel pre-processing method based on 3D morphological reconstruction [10] that enhances the background noise and limits debris. We performed 3D morphological reconstruction that preserves object boundaries, followed by multi-scale gradient and local minima elimination that limits the debris by varying the height parameter  $h$ . The parameter  $h$  used for reducing debris needs to be specified manually as its appropriate value depends on the nature of variation of gray values in the debris.

## 2.3 Background/Foreground Detection

The background/foreground detection starts with the detection of plateau minima in the gradient stack and then, labels the largest minima of height  $h$  as background and the others as foreground. At last, we applied a fast hillclimbing technique [11] on all optical slices simultaneously.

## 2.4 Cell Object Detection

This section describes the cell object detection in the image stack by region shrinking based on the Narrow Band level set (NB) approach [12] [13]. The basic idea of the narrow band level set concept is to update level sets and the driving force in a subset of points in the neighborhood of evolving front instead of the points on the grid. The narrow band has to be updated in each iteration and where it searches for closest front point over the entire fixed narrow band for computing front driving force. The time complexity of the NB method is  $O(\delta n^4)$ , where  $n$  is the number of grid points along a side and  $\delta$  is the width of narrow band. The conventional NB approach, however, is impractical for high-throughput or large scale 3D nuclei segmentation. In the proposed approach, we aim at update the level set in the nearest neighboring points (26-connected) of the deforming front points and define an appropriate speed function  $F$  that can accelerate the evolving surface to the desired object boundary.

We use an implicit representation of the surface  $S$  as the zero level set of higher dimensional time-varying function  $\Phi(S) = 0$ . The surface evolution equation as follows,

$$\frac{\partial \Phi(S)}{\partial t} = \frac{\partial S}{\partial t} \cdot \nabla \Phi + \frac{\partial \Phi}{\partial t} \Rightarrow \frac{\partial \Phi}{\partial t} = -F |\nabla \Phi| \quad (1)$$

Where  $F$  is the speed function normal to the surface  $S$ . The formulation of modified speed function is

$$F = R - \varepsilon K \quad (2)$$

Where  $R$  is an unit sign function (+1 for object region and -1 for background) that makes the object surface inflate or deflate. The signed value  $R(p)$  at pixel  $p \in D_I$  can be obtained

$$R(p) = \begin{cases} +1 & \text{if } (I(p) > T_i) \text{ then} \\ -1 & \text{Otherwise} \end{cases}, \quad T_i \in [\mu_B + k\sigma_B, \mu_{O_i} - k\sigma_{O_i}] \quad (3)$$

Here  $T_i$  is an optimal threshold value [14] between the background model  $(\mu_B, \sigma_B)$  and the candidate object model  $(\mu_{O_i}, \sigma_{O_i})$ . The viscosity term  $-\varepsilon K$  reduces the curvature of the surface. Where  $K$  is the mean curvature of the evolving surface  $S$  and  $\varepsilon$  is a non-negative regularization parameter. The mean curvature  $K$  of surface can be formulated as

$$K = \nabla \cdot \frac{\nabla \Phi}{|\nabla \Phi|} = \hat{\Delta}_x \Phi + \hat{\Delta}_y \Phi + \hat{\Delta}_z \Phi = \vec{n}_+ - \vec{n}_-,$$

where

$$\vec{n}_+ = \begin{bmatrix} \frac{D_+^x}{\sqrt{(D_+^x)^2 + (D_c^y)^2 + (D_c^z)^2 + \zeta}} \\ \frac{D_+^y}{\sqrt{(D_c^x)^2 + (D_+^y)^2 + (D_c^z)^2 + \zeta}} \\ \frac{D_+^z}{\sqrt{(D_c^x)^2 + (D_c^y)^2 + (D_+^z)^2 + \zeta}} \end{bmatrix} \quad \vec{n}_- = \begin{bmatrix} \frac{D_-^x}{\sqrt{(D_-^x)^2 + (D_c^y)^2 + (D_c^z)^2 + \zeta}} \\ \frac{D_-^y}{\sqrt{(D_c^x)^2 + (D_-^y)^2 + (D_c^z)^2 + \zeta}} \\ \frac{D_-^z}{\sqrt{(D_c^x)^2 + (D_c^y)^2 + (D_-^z)^2 + \zeta}} \end{bmatrix}$$

$D_+^x = \Phi_+^x - \Phi_c^x$ ,  $D_-^x = \Phi_c^x - \Phi_-^x$  and  $D_c^x = \frac{\Phi_+^x - \Phi_-^x}{2}$  represent forward, backward and center gradients in  $x$  direction, and similarly for  $y$  and  $z$  directions.

We utilize a FIFO queue for recursive region shrinking in depth-first order from initial foreground front points as shown in Fig.2. First, we initialize the 3D level sets  $\Phi$  with +1 for background and -1 for foreground region, and then, initialize the FIFO queue  $Q$  with the foreground points ( $\Phi = -1$ ) which have at least one outer band point (background,  $\Phi = 1$ ).

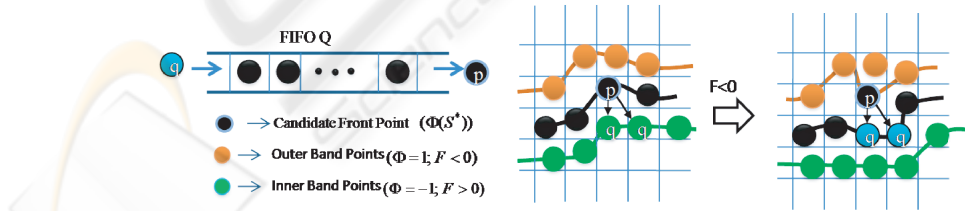


**Fig. 2.** Queue-based region shrinking at candidate front points.

In each iteration, points in the queue  $Q$  are processed, and the connected elements and object models are updated. Point  $p \in D_I$  is de-queued from queue  $Q$  one at a time and its surface driving force  $F$  is calculated as given in equation 2. If the force  $F$  is less

than zero, then the candidate point  $p$  becomes background ( $\Phi=1$ ) and its neighboring object points with level set value equal to -1 are inserted into the queue  $Q$  for recursive region shrinking process. Otherwise, if the force  $F$  at point  $p$  is greater than zero, then the candidate point  $p$  becomes cell object boundary point. This process is iterated until the criterion is satisfied. The complexity of proposed approach is linear with respect to the number of neighboring grid points. The total number of operations per iteration is bound by  $n * N_G^{26}$ , here  $N_G^{26}$  stands for 26-connected neighbors on the 3D grid and  $n$  is the number of evolving surface front points. Hence, the proposed approach limits the search range with in  $N_G^{26}$  points at each candidate surface front point against  $\delta n^2$  points for narrow band methods.

## 2.5 Marker-based Region Growing

In this section, we introduce a fast marker-based 3D region growing method for separating the merged cells that are extracted in the cell object detection step. The proposed method consists of two sequential steps, namely 3D marker detection and 3D region growing. In the marker detection step, we use conditional binary morphological erosion based on the hypothesis test followed by volume-based filtering. The proposed marker detection technique well identifies the markers in the cell object and also detects separate markers for merged cells in the image stack. The proposed 3D region growing method starts from the labeled 3D marker and then, grows the region by surface deformation, simultaneously in all the markers. We use a FIFO queue for recursive 3D region growing in depth-first order from initial 3D object markers as shown in Fig. 3.

First, we label the object markers in 3D by using connect component labeling where each marker get unique label and then, initialize the 3D level sets  $\Phi$  with +1 for background and -1 for 3D object marker and the FIFO queue  $Q$  with the outer band points (Background,  $\Phi=1$ ) which have at least one marker object point (Marker,  $\Phi=-1$ ).

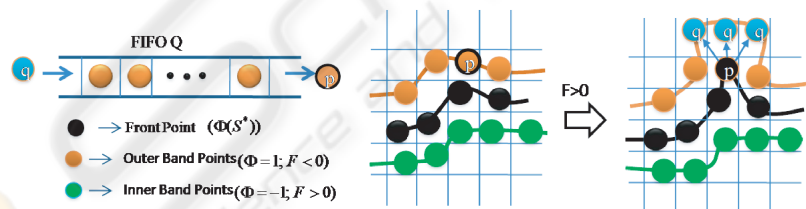


Fig. 3. Queue-based region growing at candidate outer points.

Outer band point  $p \in D_I$  is de-queued from queue  $Q$  one at a time and its surface driving force  $F$  is calculated as given in equation 2. If the force  $F$  at point  $p$  is greater than zero, then we decide the label of candidate point  $p$  based on its neighboring surface front points. If the candidate  $p$  has neighboring surface front points which are originated from same marker, then the outer band point  $p$  becomes surface front point and its neighboring outer band points  $q \in N_G(p)$  with level set value equal to 1 are inserted into the queue  $Q$  for recursive region growing process. However, if the point  $p$

has surface front neighbors which are originated from different markers, then, the point  $p$  gets a watershed label which is used to separate the adjacent surface fronts. Otherwise, if the force  $F$  at point  $p$  is less than zero, then, the candidate point  $p$  becomes background. The present iteration completes when all the points in the queue visited. In the each iteration, we update the object models. This process is iterated until the criterion is satisfied. Finally, we apply an isotropic and discrete Gaussian shape filter of size  $(3 \times 3 \times 3)$  on the 3D level set for smoothening the surface points.

### 3 Experimental Results

We performed a set of experiments to evaluate the proposed 3D segmentation method for the detection of cell nuclei in Live *Drosophila* Embryos time-lapse images. We tested our segmentation on image stacks acquired during different stages of embryonic development; the synchronous nuclear cycles of the syncytial blastoderm and mitotic domains of the post-cellular blastoderm that contain mixtures of different phases of the cell cycle. Figure 4 illustrates the experimental results obtained from applying the proposed 3D segmentation method for post-cellular blastoderm time-lapse images. The method has been evaluated by manually creating ground truth, developed by automatic thresholding on image stack followed by manual correction on individual cells by using ImageJ plugin. We evaluated the segmentation results based on the object level accuracy such as number of correctly classified cells, merged cells and split cells, and pixel level detection rates, namely miss detection rate and false alarm rate. The accuracy of our approach was evaluated for image data recorded during different stages of development (Table 1). On average, 96% of 3D cell nuclei were identified. The segmentation quality on the pixel level ranged between 85%-90%. Figure 5 shows a mitotic nucleus track from interphase to the end of anaphase in wildtype syncytium.

**Table 1.** The performance of proposed method in Live *Drosophila* Embryos time-lapse images.

Image Stack (70 slices)	No. of cell nuclei	Object level accuracy			Pixel level	
		Correct cells	Merged cells	False Positives	Split cells	Accuracy
Post-cellular blastoderm	192	187	1	13	6	86.45%
Syncytial blastoderm	96	96	0	1	0	88.67%

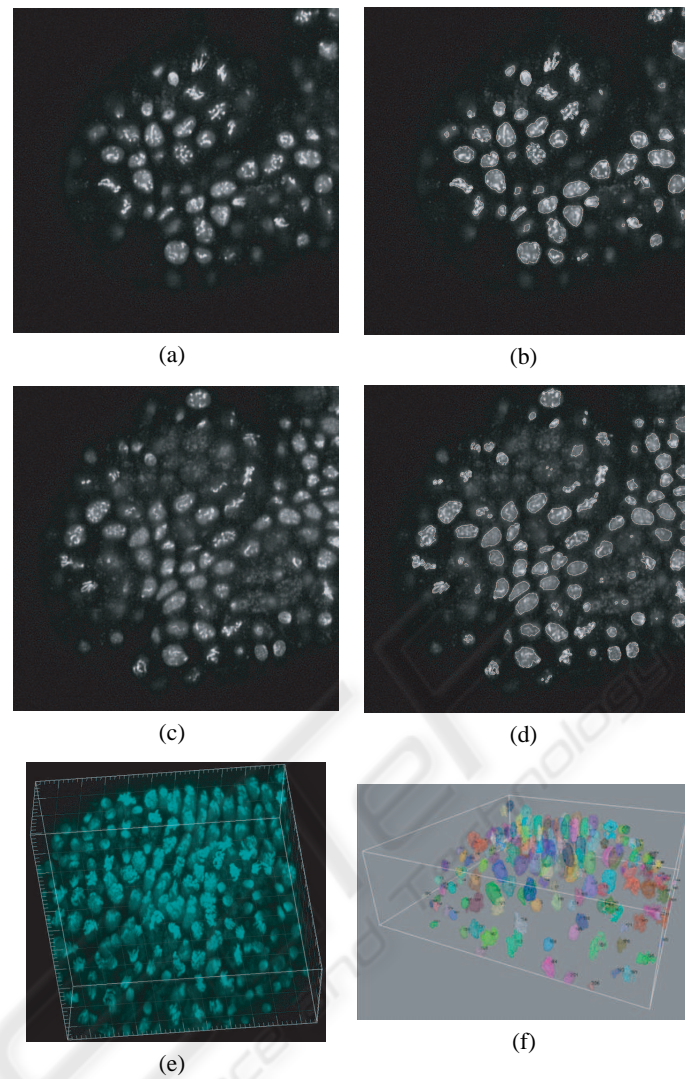


**Fig. 4.** Automatic segmentation of cell nuclei in images acquired during the post-cellular blastoderm of embryogenesis. (a) Original optical slice 15, (c) original optical slice 25, (e) Maximum Intensity Projection (MIP) of original image stack. Segmentation results of optical slices 15 (b) and 25 (d). Contours of detected regions of interest are shown in white. (f) 3D visualization of segmented cell nuclei and their labels.

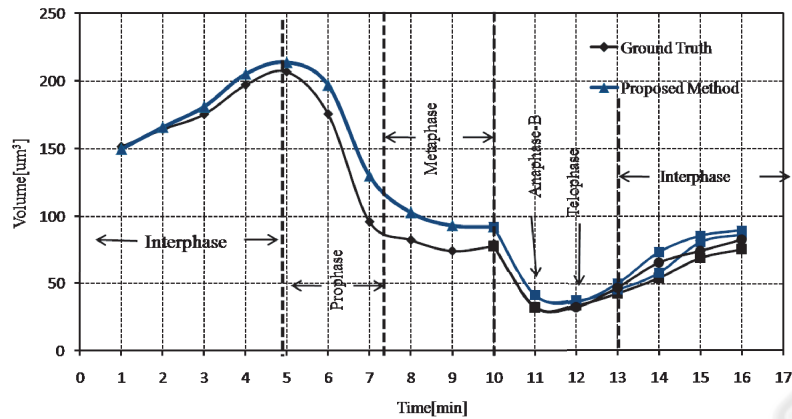


**Fig. 5.** Cell cycle dependant changes of nuclear and chromosomal volume from interphase to the end of anaphase in wildtype syncytium.

## 4 Conclusions

We presented a novel method for the detection of fluorescently labeled cell nuclei in 3D image stacks. Reliable segmentation of cell nuclei and mitotic chromosomes is very important for the study of cell cycle progression in Live *Drosophila* Embryo. We introduced a methodology based on narrow band level sets for isolating the cell nuclei from background. The proposed method has been evaluated regarding object level and pixel level accuracy. Preliminary results show that the outputs of the image segmentation are suitable for downstream tracking, quantification and classification of identified image objects.

## References

1. Garcia, K., Duncan, T., Su, T.: Analysis of the cell division cycle in drosophila. *Methods* 41 (2007) 198–205
2. Adiga, P.S.U., Chauduri, B.B.: An efficient method based on watershed and rule-based merging for segmentation of 3-D histo-pathological images. *Pattern recognition* 34 (2001) 1449–1458
3. Li, G., Umesh Adiga, Olson, K., John, F., Guzowshi, Barnes, C.A., R. Badrinath: A hybrid 3D watershed algorithm incorporating gradient cues and object models for automatic segmentation of nuclei in confocal image stacks. *Cytometry A* 56A (2003) 23–36
4. Gang Li, Chawala, M., Olson, K., Guzowski, J., Barnes, C., R. Badrinath: Hierarchical, model-based merging multiple fragments for improved three-dimensional segmentation of nuclei. *Cytometry A* 63A (2005) 20–23
5. Gang Li, Tianming Liu, Ashley T., Jingxin Nie, Guo, L., Mara, A., Holley, S., Stephen T C Wang: 3D cell nuclei segmentation based on gradient flow tracking. *BMC Cell Biology* 8 (2007)

6. Dufour A., Shinin V., Tajbaksh S., Guillen N., Olivo-Marin J., Zimmer C.: Segmenting and tracking fluorescent cells in dynamic 3D microscopy with coupled active surfaces. *IEEE Transactions on Image Processing* 14 (2005)
7. A, D., JooHyun Lee, Nicole Vincent, Grailhe, R., Auguste Genovesio: 3D automated nuclear morphometric analysis using active meshes. In: *Pattern recognition in Bioinformatics*. Volume LNBI4774. (2007) 356–367
8. Clarkson, M., R., S.: A His2AvDGFP fusion gene complements a lethal His2AvD mutant allele and provides an in vivo marker for drosophila chromosome behavior. *DNA and Cell Biology* (1999)
9. Silvia Cermelli, Yi Guo, Steven P. Gross, Michael A. W.: The lipid-droplet proteome reveals that droplets are a protein-storage depot. *Current Biology* 16 (2006) 1783–1795
10. Wang, D.: A multiscale gradient algorithm for image segmentation using watershed. *Pattern Recognition* 30 (1997) 2043–2052
11. Rambabu, C., Chakrabarti, I.: An efficient hillclimbing-based watershed algorithm and its prototype architecture. *Journal of signal processing systems* 52 (2008) 281–295
12. L., C.D.: Computing minimal surfaces via level curvature flow. *Journal of Computational Physics* 106 (1993) 77–91
13. Paragios N, Deriche R: Geodesic active contours and level sets for the detection and tracking of moving objects. *IEEE Trans. On PAMI* 22 (2000) 266–280
14. H. -S. Wu, Barba J., Gil J.: Iterative thresholding for segmentation of cells from noisy images. *Journal of microscopy* 197 (2000) 296–304

